Anal. Chem. **2004,** *76,* 1249−1256

Direct Chemical Analysis of Solids by Laser Ablation in an Ion Storage Time-of-Flight Mass Spectrometer

Gregory L. Klunder,*,† Patrick M. Grant,† Brian D. Andresen,† and Richard E. Russo‡

Forensic Science Center, Lawrence Livermore National Laboratory, Livermore, California 94551, and Lawrence Berkeley National Laboratory, Berkeley, California 94720

A laser ablation/ionization mass spectrometer system is described for the direct analysis of solids, particles, and fibers. The system uses a quadrupole ion trap operated in an ion storage mode, coupled with a reflectron time-of-flight mass spectrometer). The sample is inserted radially into the ring electrode, and an imaging system allows direct viewing and selected analysis of the sample. Measurements identified trace contaminants of Ag, Sn, and Sb in a Pb target with single laser shot experiments. Resolution ($m/\Delta m$) of 1500 and detection limits of ~10 pg have been achieved with a single laser pulse. The system configuration and related operating principles for accurately measuring low concentrations of isotopes are described.

Direct chemical analysis of solids without chemical pretreatment can offer many advantages for the analytical chemist. Elimination of chemical solvents and wastes, reduced sample handling, and faster analysis times are some of the motivations for developing such techniques. Laser ablation is one of the leading areas being investigated for direct solid sample analysis. Focusing a short pulse laser beam onto a sample will create an explosion that produces atoms, ions, clusters, and particles[1−3] for direct analysis by mass or optical spectrometry or introduction into an ICPMS. The spatial resolution of the laser beam makes this an excellent technique for interrogating single particles. However, excellent detection sensitivity is required due to the limited absolute mass and concentration from a micrometer-sized particle.

Laser ablation ionization for direct introduction into a mass spectrometer has been reviewed in several excellent references.[4,5] Numerous types of mass spectrometers have been used for detection, including time-of-flight, Mattauch−Herzog, magnetic sector, FT-MS, quadrupoles, and ion traps. Most of these systems have used external ablation/ionization followed by aerosol introduction into the mass spectrometer. Laser ablation has also been performed inside the cavity of an ion trap for direct mass spectrometric analysis of bulk and particulate samples. Gill and Blades investigated the ablation of metals, ceramics, and polymers inside the ion trap, demonstrating the capability to perform atomic and molecular mass spectrometry.[6,7] Gill et al. followed by demonstrating the power of resonant laser ablation for selective ablation/ionization of metals in the ion trap.[8] Ramsey et al. demonstrated the capability of ablating single droplets (or particles) injected into an ion trap.[9,10] Song et al. applied laser ablation inside an ion trap mass spectrometer for the analysis of rare-earth elements in soil samples with scans averaged 100 times.[11]

Although the ion trap functions as a scanning mass spectrometer, it can also be used as a storage device for preconcentration of ions as a front end for injection into a time-of-flight mass spectrometer (TOF-MS).[12] The ion trap can store a large range of masses or be used to selectively store narrow mass regions, thus reducing background interferences from sample matrixes. However, the ion trap is limited by the number of ions that can be stored and by space-charge effects. When high resolution over a large mass range is required, the scan times can be lengthy and may be a limiting factor for some applications. TOF spectrometers provide excellent resolution of short pulse injected ions over extended mass ranges. These instruments can use gated sample introduction but are incapable of ion storage and accumulation. Lubman et al. developed the hybrid ion storage (IS)-TOF-MS, which takes advantage of the storage capabilities of the ion trap and the speed and resolution of the time of flight.[13,14]

* To whom correspondence should be addressed. E-mail: klunder@llnl.gov.
† Lawrence Livermore National Laboratory, Livermore, CA.
‡ Lawrence Berkeley National Laboratory, Berkeley, CA.

(1) Russo, R. E.; Mao, X.; Mao, S. *Anal. Chem.* **2002**, *74*, 71A−77A.
(2) Russo, R. E. *Appl. Spectrosc.* **1995**, *49*, 14A−28A.
(3) Miller, J. C.; Haglund, R. F., Jr., Eds. *Laser Ablation and Desorption, Experimental Methods in the Physical Sciences*,; Academic Press: New York, 1998; Vol. 30.
(4) Vertes, A.; Gijbels, R.; Adams, F. *Laser Ionization Mass Analysis*; J. Wiley & Sons: New York, 1993.
(5) Lubman, D. M., Ed. *Lasers and Mass Spectrometry*,; Oxford University Press: New York, 1990.
(6) Gill, C. G.; Blades, M. W. *J. Anal. At. Spectrosc.* **1993**, *8*, 261−267.
(7) Gill, C. G.; Daigle, B.; Blades, M. W. *Spectrochim. Acta, B* **1991**, *46*, 1227−1235.
(8) Gill, C. G.; Garrett, A. W.; Hemberger, P. H.; Nogar, N. S. *Spectrochim. Acta, B* **1996**, *51*, 851−862.
(9) Dale, J. M.; Yang, M.; Whitten, W. B.; Ramsey, J. M. *Anal. Chem.* **1994**, *66*, 3431−3435.
(10) Gieray, R. A.; Reilly, P. T. A.; Yang, M.; Whitten, W. B.; Ramsey, J. M. *Anal. Chem.* **1998**, *70*, 117−120.
(11) Song, K.; Cha, H.; Lee, J.; Park, H.; Lee, S. C. *Microchem. J.* **2001**, *68*, 265−271.
(12) March, R. E.; Hughes, R. J. *Quadrupole Storage Mass Spectrometry*; J. Wiley & Sons: New York, 1989.
(13) Chien, B. M.; Michael, S. M.; Lubman, D. M. *Int. J. Mass Spectrom. and Ion Processes* **1994**, *131*, 149−179.

10.1021/ac0303261 CCC: $27.50 © 2004 American Chemical Society
Published on Web 01/24/2004

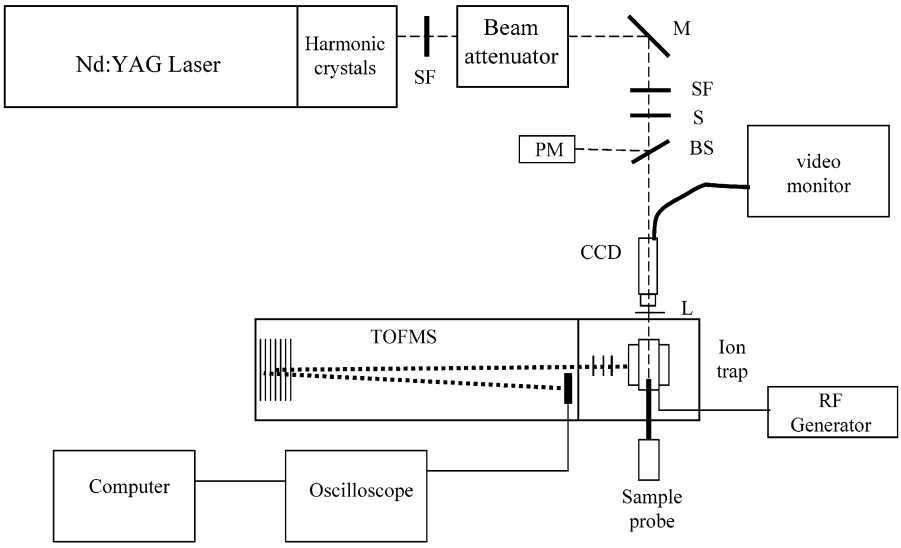

Figure 1. Block diagram of the experimental configuration: SF, spatial filters; M, mirror; S, shutter; BS, 90/10 beam splitter; L, focusing lens; PM, power meter.

This instrument has been applied to a number of methods including matrix-assisted laser desorption/ionization.

The goal of our research is to determine the chemical composition of very small samples, including micrometer-sized particles. The spatial resolution capable with laser ablation makes this a good source for ionization, while the sensitivity and versatility of the IS-TOF-MS make it an ideal detector for analyzing small samples. In this work, we describe an instrument configuration that uses laser ablation inside an IS-TOF-MS, with an imaging system to visually screen and select particles for analysis. The laser beam focused onto the target induces vaporization and direct ionization of the sample.

EXPERIMENTAL SECTION

The IS-TOF-MS system in our laboratory has been previously described.[15,16] However, significant modifications have since been incorporated, and they are described here. Figure 1 shows a block diagram of the system, and Table 1 summarizes the operating conditions. The laser used for ablation/ionization was the third harmonic (λ = 354 nm, pulse width ~10 ns) of a Nd:YAG laser (Quanta-Ray GCR-130), which was operated at full power for optimum stability. A variable attenuator (Newport, model 935-10) and a 90/10 beam splitter (CVI Laser Optics) were used to reduce the laser energy. A power meter (Ophir Nova with a model PE-10 detector head) was calibrated and used to monitor the energy of each laser pulse after the 90% splitter. A final single lens (CVI Laser Optics), with a focal distance of 70.8 mm, was situated on an x−y-z translation stage directly in front of the quartz window of the vacuum chamber to steer and focus the beam onto the target. The laser spot size was determined by several methods: burn paper, calculations, and crater diameter. The spot size measured by placing burn paper in the sample position was determined to be ~26 μm in diameter. However, this value could be slightly high due to the sensitivity of the paper and position of the beam focus. The calculated diffraction limited spot size was ~16 μm. However, crater diameters were measured as small as 10 μm. Spot size was determined after ablation by measuring the crater diameter with a white light microscope (Zygo, model New View 100). Figure 2 shows the timing diagram for the rf trapping and laser firing. The flash lamps pumping the laser were externally triggered in order to synchronize them with the rf of the trap. A delay time was set with respect to the rf phase and cycle number using a delay generator (Stanford Research Systems, model DG-535). The laser was operated repetitively, and pulses for ablation were selected with a shutter. This procedure was more stable than firing the laser in single-shot mode. A fast photodiode (ElectroOptics Technology, model ET-2000) was used to monitor the phase when the laser was fired.

Table 1. Summary of the Operating Parameters of the Laser Ablation IS-TOF-MS System

Laser	
wavelength	354 nm
pulse width	10 ns
energy	10−100 μJ
rep rate	10 Hz
spot size	16−30 μm
Ion Trap	
rf potential	300 Vp-p
pressure	10^{-4} Torr
fill gas	helium
end cap ejection	± 900 V
XY1	−1179 V
XY2	−1115 V
focusing optic	−776 V
rf frequency	1.0 MHz
rf clamp time	200 μs
storage time	0.002−99.8 ms
Time-of-Flight	
flight tube liner	−1246 V
reflectron front	−304 V
reflectron back	+376 V
microchannel plate	−1545 V
pressure	10^{-6} Torr

(14) Qian, M. G.; Lubman, D. N. *Anal. Chem.* **1995**, *67*, 234A.
(15) Russo, R. E.; Klunder, G. L.; Grant, P.; Andresen, B. D. *Appl. Phys. A* **1999**, *69*, S895−S897.
(16) Chambers, D. M.; Grace, L. I.; Andresen, B. D. *Anal. Chem.* **1997**, *69*, 3780−3790.

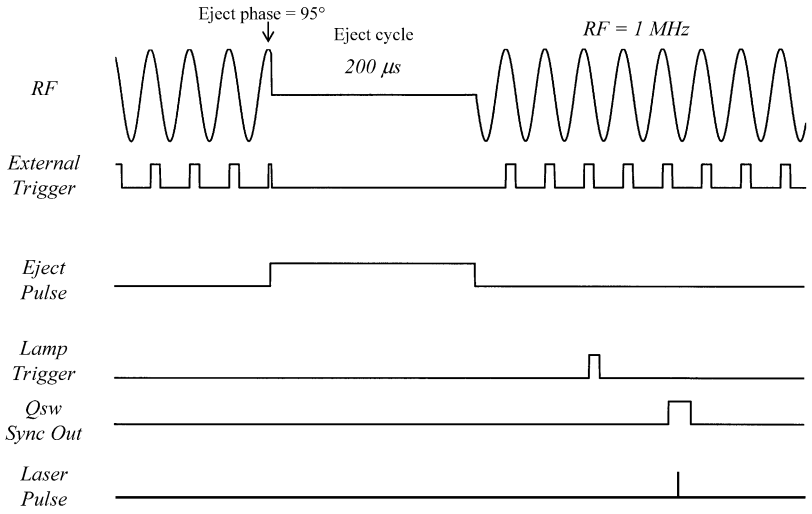

Figure 2. Timing diagram of the IS-TOF-MS experiment. Firing the laser was synchronized with the rf potential.

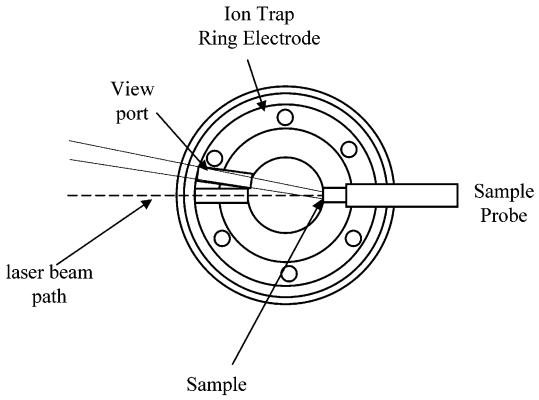

Figure 3. Ion trap ring electrode showing the alignment of the sample, laser beam, and view port.

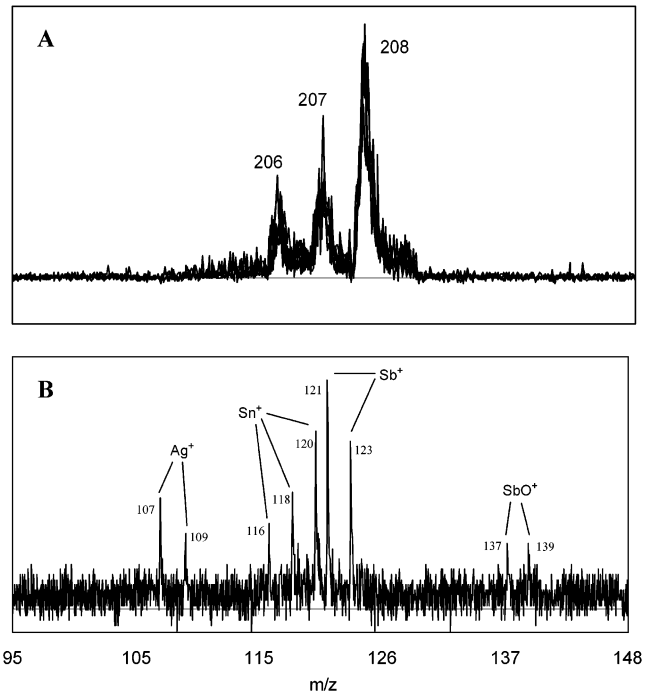

Figure 4. (A) Mass spectra showing reproducibility of the abundance of the primary Pb isotopes for five separate laser pulses at five locations on a Pb foil. (B) Trace impurities in the Pb sample were identified from a single-laser pulse. The laser beam spot size was ~12 μm, which provides an irradiance of ~1 GW/cm^2.

The ring electrode of the ion trap (Finnigan) was modified by drilling three small holes to accommodate the sample, the laser beam, and sample imaging. Two holes were placed 180° apart, and the third was placed off-axis of these two holes (Figure 3). A Plexiglas probe with a sample on the tip surface (3 mm in diameter) was inserted directly into the center ring of the ion trap. The laser beam enters the trap on the probe axis, at 180° to the probe. A CCD camera/microscope (HiScope compact microvision system, model KH 2200 MD2 with MX 400 lens and L-8 × 8 cm extender) is slightly off-axis from the laser and allows on-line sample viewing inside the ion trap. The sample is illuminated through a window in the top of the vacuum chamber. The Plexiglas sample probe acts as a light pipe for back-illumination, while front illumination was achieved by light reflected from surfaces on the inside of the trap.

The optimum ejection phase of ions into the TOF was previously determined by Chambers et al. to be 95°.[16] An rf power supply (RM Jordan, model D-1240) provided voltage to the ring electrode at 1-MHz frequency during the storage cycle. Special electronic circuits for rapid clamping and restoring the rf voltage were designed and fabricated in our laboratory. At the time of ejection, the end-cap electrodes were switched from ground to +900 and −900 V with HV transistor switches (Behlke, model HTS 31-GSM). An e-gun (RM Jordan) was used for electron impact ionization of PFTBA as calibrant gas. The ion trap/sample chamber was back-filled with He to 10^{-4} Torr, and the reflectron TOF-MS was maintained at 10^{-6} Torr.

The time-of-flight instrument (RM Jordan, model D-850) was 1 m long with a linear reflectron and dual microchannel plate detector. The flight tube was biased at −1200 V, and the reflectron voltages were 380 and −250 V for the front and back stages, respectively. The microchannel plates were biased with −1280 V, evenly divided. Prior to each experiment, the system was calibrated with PFTBA. Peak shape, resolution, and linearity over the mass range were measured and compared to results obtained without the geometric modifications of the ion trap. No apparent limitations or distortions due to the holes were observed for trapping ions based on mass spectra measured for PFTBA.

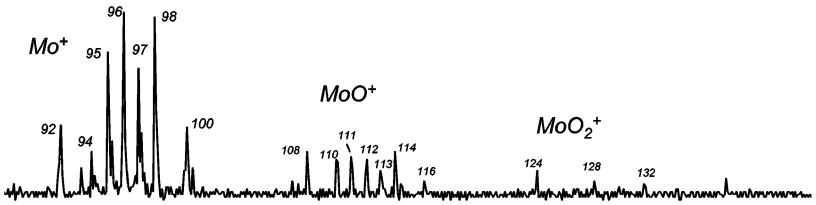

Figure 5. Mass spectrum from the first laser pulse on a molybdenum foil target with 10 μJ with a 15-μm-diameter spot.

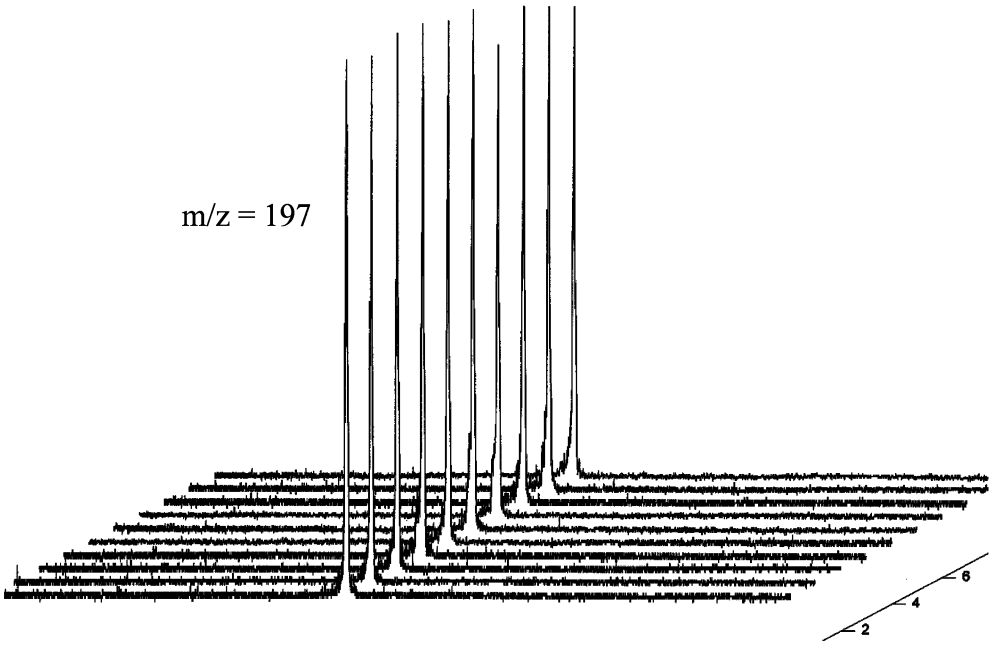

Figure 6. Mass spectra from 10 consecutive laser pulses on a gold foil target resulting in a reproducibility of ~2% based on peak area calculations. The laser was fired during the middle of the storage cycle, with storage time ~49 ms. The pulse energy was ~22 μJ and the spot size ~10 μm.

Linearity and resolution were typically 0.999 99 ($m/z = \alpha t^2 + \beta$) and 1500, respectively.

Data acquisition was achieved with a digital storage oscilloscope (Lecroy 9360) which used an 8-bit ADC capable of digitizing 5 Gs/s at a 600-MHz bandwidth. In-house software written with LabView (National Instruments) was used to control the shutter and collect data from the oscilloscope via GPIB. The flight time data were converted to mass/charge based on calibration with the PFTBA standard. The data were imported into other software packages (Galactic Grams32/AI software or Microsoft Excel) for analysis.

Scanning electron microscope foil grids (Ted Pella, Inc.), cut to appropriate size to fit on the probe tip, were used as the metal samples. The Pb sample was laboratory lead tape. The glue used to hold the sample on the probe tip was a contact adhesive (3M Fastbond, 30-NF) that we have characterized by this method. Samples used in this study were relatively large, and no contributions from the adhesive were observed.

RESULTS AND DISCUSSION

Figure 4A shows the mass spectra from ablation of a Pb target using five consecutive laser pulses of 10 μJ/pulse with a crater diameter of 12 μm; the irradiance was ~1GW/cm^2. The mass resolution was ~1500 ($\Delta m/m$), and the peak areas were reproducible to 4−5%. The laser was fired during the middle of the rf storage cycle for a total storage time of 49 ms. With the exception

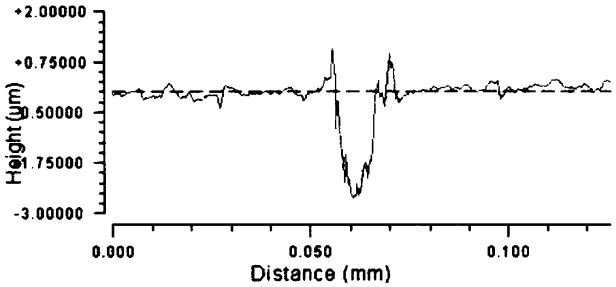

Figure 7. Crater profile from the ablation of a gold target by five laser pulses. Pulse energy ~10 μJ; spot size ~10 μm.

of the ^{204}Pb isotope, which was not clearly detected in single-pulse experiments, the primary natural isotope ratios of lead, 206 (23.6% natural abundance), 207 (22.6%), and 208 (52.3%), were well resolved.[17] The measured abundances were determined to be 19.9, 24.9, and 55.2%, respectively. However, further improvements in resolution with energy focusing could further improve the isotope ratios. For single-pulse experiments, a crater depth could not be measured due to the small quantity of material removed and the relatively rough surface of the Pb target. Figure 4B shows a different portion of the mass spectrum in one of the traces of Figure 4A. The mass peaks correlate to Ag 107 (51.8% natural

(17) Weast, R. C., Ed. *Handbook of Chemistry and Physics*, 64th ed.; CRC Press: Boca Raton, FL, 1984.

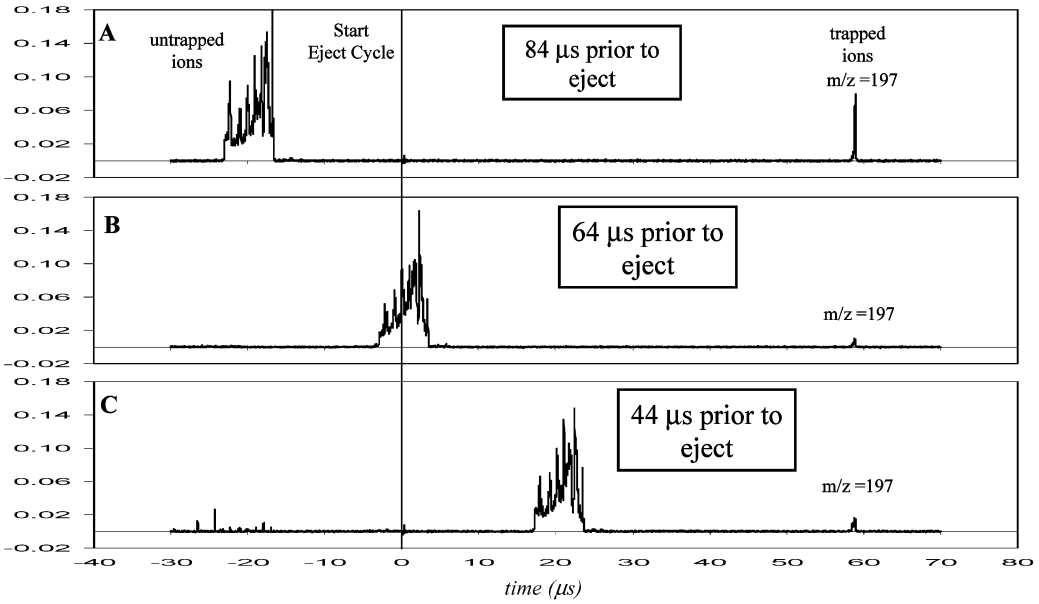

Figure 8. Ablation of gold foil sample with longer delays of the laser pulse (i.e., shorter storage times). Flight time for large ion cloud ~59 μs from laser pulse. Laser pulse energy ~25 μJ; ejection phase 0°, $n = 3$.

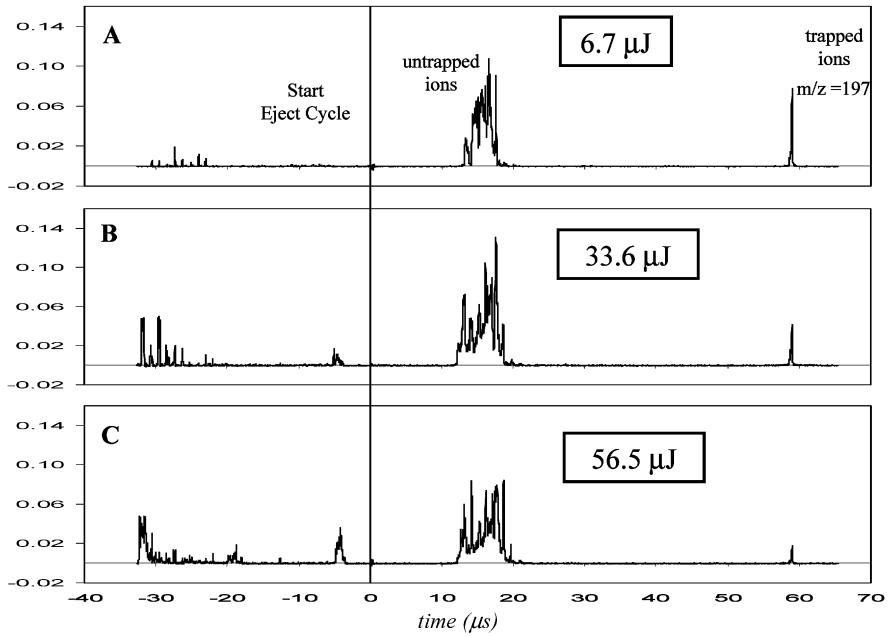

Figure 9. Ablation of gold foil sample with increasing laser power. Laser pulse 46 μs prior to eject cycle; ejection phase 0°, $n = 3$.

abundance) and 109 (48.2%), Sn 116 (14.5%),118 (24.2%), and 120 (32.6%), and Sb 121 (57.3%) and 123 (42.7%), which are common contaminants typically found in Pb at parts-per-thousand levels. Other minor isotopes of Sn were not detected: 114 (0.65%), 115 (0.36%), 117 (7.7%), 119 (8.6%), 122 (4.6%), and 124 (5.8%). Two small peaks, which appear at m/z 137 and 139, could be attributed to SbO; however, they are not significantly above the background. The data in Figure 4 demonstrate the capability of this technique for analyzing bulk material to measure trace elements with a single laser pulse.

Figure 5 depicts the mass spectrum from the first laser pulse on a molybdenum target and identifies molybdenum oxides as well as the Mo^+ isotopes. The oxides were observed only in the first pulse, and subsequent pulses at the same location resulted in only the Mo^+ isotope distribution. Although, depth profiling was not the focus of this study, this experiment clearly demonstrated the capability of performing surface analysis on the sample.

Figure 6 shows 10 consecutive mass spectra from the ablation of a gold foil target; gold was chosen because it is monoisotopic. Peak areas were reproducible to ~2%. A typical crater profile for five ablation pulses on the gold target is shown in Figure 7. This profile was representative of normal observations of the ablation of metals and alloys with ns laser pulses.[2] The rim is due to splashing resulting from the melting process. Assuming a cylindrical geometry with a diameter of 11 μm and depth of 2.5 μm, the total volume was ~240 μm^3. Based on a density of 10 g/mL, this volume correlated to ~2 ng of total mass ablated or 0.4 ng/pulse. However, that result is mass removed from the crater but does

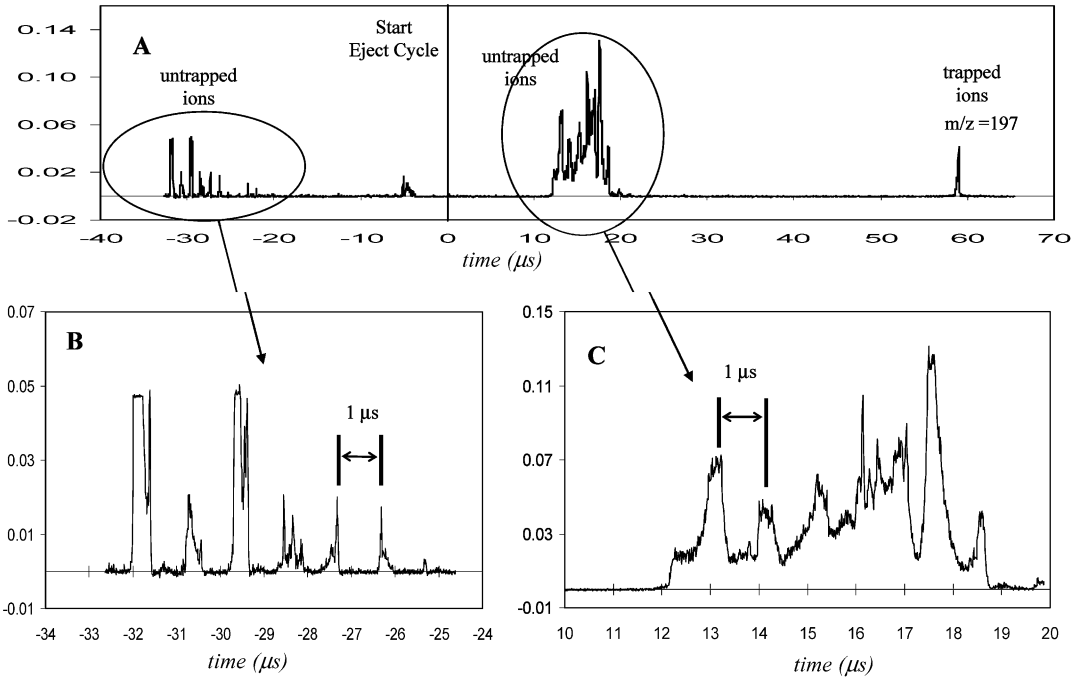

Figure 10. Expanded view of Figure 9B showing the influence of rf on the ion clouds. Laser pulse energy ~34 μJ, 46 μs prior to eject cycle; ejection phase 0°, $n = 3$.

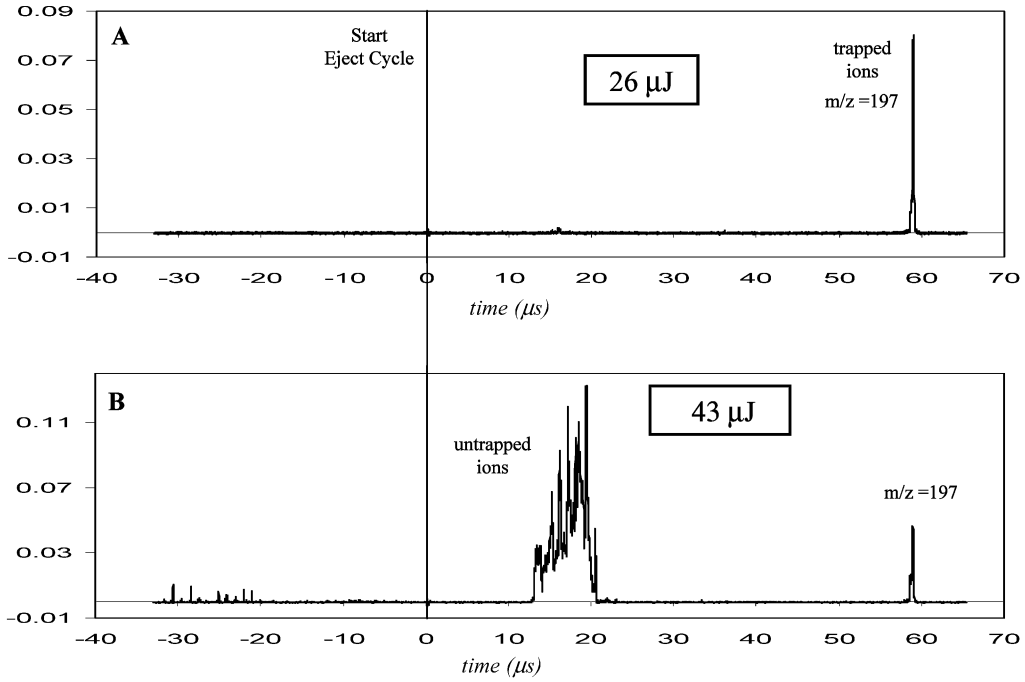

Figure 11. Experimental conditions are the same as for Figure 8, with a slightly larger spot size. (A) 26 μJ; (B) 43 μJ.

not consider any mass that may be redeposited on the surface or was contained in the rim volume. A rough order of magnitude calculation of the rim volume, estimated a value of ~40 μm^3, which is a significant fraction of the total crater volume. Although, only rough estimates, these calculations indicated that the sensitivity of this instrument for a single laser pulse was on the order of picograms. Similar values were obtained for other metal foil targets. For the case of the lead sample in Figure 4, detection of the trace contaminants indicated that the sensitivity of the method may be on the order of femtograms.

The ion storage times were adjusted by varying the firing of the laser with respect to the rf cycle of the trap (see Figure 2). Figure 8 shows the results of reducing the storage times and firing the laser closer to the eject cycle. The trigger on the scope was offset to display the detector output prior to the ejection pulse, as indicated by the negative time data. At 84-μs storage time (Figure 8A), a large packet of ions reached the detector ~24 μs prior to the eject cycle. The ~59-μs delay of the appearance of the ion clouds corresponded to the signal for the flight time of the trapped gold ions. The flight time for untrapped ions remained constant

as the storage time was reduced to 64 (B) and 44 μs (C); the large ion packet shifted by the same amount. This large ion packet is due to gold ions that were generated by the laser ablation pulse but not stored in the ion trap. Gold ions that were trapped and ejected appeared consistently at 59 μs. The width of the large ion packet is attributed to the kinetic energy and spatial distributions of the laser-generated ions. Based on peak area measurements, the trapped ions observed at 59 μs represented only 4% of the ions generated during the ablation process.

Figure 9 shows that even when laser power was reduced to ~6.7 μJ, a large number of ions were generated, but only a small fraction of which were trapped. Increasing the laser power increased the number of ions generated, as measured by the peak areas of the untrapped ions, although not necessarily the trapped ions. The decrease in trapped ion intensity is likely due to generating more ions with greater kinetic energy and fewer ions that can be trapped by the potential well under these storage conditions. Increasing laser energy from 6.7 to 33.6 μJ resulted in a 50% increase in total area. However, the measured area decreased slightly when the laser energy was increased from the 33.6 to 56.5 μJ. The loss was perhaps attributed to ions outside the window of the oscilloscope settings. The laser was fired 46 μs prior to the eject cycle, and untrapped ions reached the detector 14 μs after ejection. With increased laser power, another cloud of ions reached the detector more quickly. These ions had a higher kinetic energy and therefore traveled down the flight tube much faster. The two kinetic energy distributions is consistent with other measurements of ion clouds generated by laser ablation and measured by TOF-MS.[18,19] The untrapped ions appeared to be affected by the rf potential, as shown in Figure 10. The ion clouds exhibited a periodicity that matched the 1-MHz frequency of the rf applied to the ring electrode. One theory is that the ions do not penetrate the field created by the rf but instead traverse the periphery of the field being preferentially ejected by the field force. Alternatively, the cloud of ions could move through the center of the trap with the rf field attempting to put them into orbit within the trap. Some ions are extracted as the clouds move past the TOF inlet while some with the proper kinetic energy are trapped. The kinetic energy distribution of laser ablation-generated ions is large compared to those generated by laser desorption. Previous papers have emphasized the importance of temporal considerations of laser firing with respect to phase and trapping efficiency of laser-desorbed ions.[20,21] In these studies, varying the phase of the laser firing did not result in such dependence. However, this observation was perhaps due to trapping a limited kinetic energy range of the ablated ions that have a broad kinetic energy distribution.

Figure 11 demonstrates that increasing the laser beam spot size (reducing fluence) significantly improved the trapping efficiency. In Figure 11A, a slightly larger spot size was used relative to the experiment of Figure 9. The laser fluence was closer to the ablation threshold, and therefore, more ions of lower kinetic energy were produced. Most of these ions fell into the potential well of the ion trap, and untrapped ions were thus not observed. Laser ablation is a nonlinear process and increasing laser power above the ablation threshold can therefore significantly increase ionization. When the power was then increased at this same spot size, a large number of untrapped ions were again observed (Figure 11B). Increasing the rf potential should increase the effectiveness of the trap by increasing the depth of the potential well. The results of this experiment with a molybdenum target are shown in Figure 12. As the rf potential was increased, untrapped ions were slowed and more of them were extracted into the TOF. Another observed effect was reduction of the number of trapped Mo^+ ions, as would be expected since they were essentially being tuned out of the trap. The trapping and storage efficiency of laser-generated ions should be improved by incorporating dynamic trapping routines, as demonstrated by Eiden et al.[22,23] Although the holes in the ring electrode may distort the rf field and alter the trapping potential, no deleterious effects were observed with the PFTBA calibrant gas with this atypical configuration. This fact argues against the holes as a primary cause for untrapped laser-ablated ions.

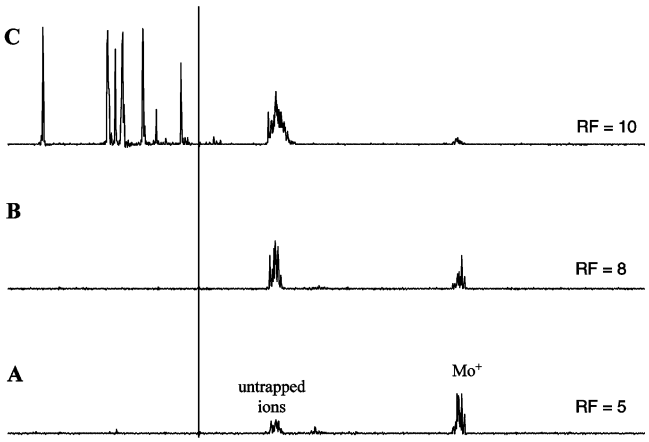

Figure 12. Influence of increasing rf potential on the untrapped ions generated from a Mo target.

CONCLUSION

We have demonstrated some useful capabilities of performing laser ablation of materials in an ion storage time-of-flight mass spectrometer. The reproducibility and sensitivity of this system can provide reliable chemical information on very small samples. The imaging system provided good spatial resolution and an ability to guide the laser beam to a specific location on a target sample, including a single micrometer-sized particle. Generating ions by laser ablation directly inside an ion trap minimizes transport losses and allows better absolute mass detection limits. The current detection limits were estimated to be in the picogram to femtogram range from the mass removed by the ablation crater. Although the instrument sensitivity can be improved, more work will be necessary to optimize the ionization and trapping efficiencies. Selected ion storage and multiple laser pulses per ejection will result in lower concentration limits of detection.

(18) Kelly, M. C.; Gomlak, G. G.; Panayotov, V. G.; Cresson, C.; Rodney, J.; Koplitz, B. D. *Appl. Surf. Sci.* **1998**, *127−129*, 988−993.
(19) Fukushima, K.; Kanke, Y.; Morishita, T. J. *Appl. Phys.* **1993**, *74*, 6948−6952.
(20) Robb, D. B.; Blades, M. W. *Int. J. Mass Spectrom.* **1999**, *190/191*, 69−80.
(21) Robb, D. B.; Blades, M. W. *Rapid Commum. Mass Spectrom.* **1999**, *13*, 1079−1087.
(22) Eiden, G. C.; Garrett, A. W.; Cisper, M. E.; Nogar, N. S.; Hemberger, P. H. *Int. J. Mass Spectrom. Ion Processes* **1994**, *194*, 119−141.
(23) Eiden, G. C.; Cisper, M. E.; Alexander, M. L.; Hemberger, P. H.; Nogar, N. S. *J. Am. Soc. Mass Spectrom.* **1993**, *4*, 706−709.

ACKNOWLEDGMENT

The authors gratefully acknowledge the members of the LLNL FSC for their contributions to this work, especially David Chambers and Louis Grace. The work was supported by the Department of Energy, Office of Nonproliferation and National Security, NA22, through the Lawrence Livermore National Laboratory, Contract W-7405-ENG-48, and through the Lawrence Berkeley National Laboratory, Contract DE-AC03-76SFOO098.

Received for review September 9, 2003. Accepted December 15, 2003.

AC0303261